# Enhanced Hygrothermal Stability of In-situ Grown $MAPbBr_3$ Nanocrystals in Polymer with Suppressed Desorption of Ligands

*Hui Fu[ab], Kai Wang[a], Hao Wu[a], Chris R. Bowen[c], Zhi Fang[a], Zebin Yan[a], Shuheng Jiang[a], Deliu Ou[a], Yang Yang[a], Jinju Zheng[ab,]*, and Weiyou Yang[ab,]**

[a] Institute of Micro/Nano Materials and Devices, Ningbo University of Technology, Ningbo City, 315211, P. R. China.

[b] Zhejiang Institute of Tianjin University, Ningbo, Zhejiang 315201, China

[c] Department of Mechanical Engineering, University of Bath, BA2 7AK, UK.

KEYWORDS: perovskite, nanocrystal, ligand modification, hygrothermal stability, optical property

ABSTRACT: Currently, the intrinsic instability of organic−inorganic hybrid perovskite nanocrystals (PNCs) at high temperature and high humidity still stands as a big barrier to hinder their potential applications in optoelectronic devices. Herein, we report the controllable in-situ-grown PNCs inpolyvinylidene fluoride (PVDF) polyme with profoundly enhanced hygrothermal stability. It is found that the introduced tetradecylphosphonic acid (TDPA) ligand enables significantly improved binding to the surface of PNCs via a strong covalently coordinatedP−O−Pb bond, as evidence by density functional theory calculations an X-ray photoelectron spectroscopy analyses. Accordingly, such enhanced binding could not only make efficient passivation of the

surface defects of PNCs but also enable the remarkably suppressed desorption of the ligand from the PNCs under high-temperature environments. Consequently, the photoluminescence quantum yield (PL QY) of the as-fabricated $MAPbBr_3$−PNCs@PVDF film exhibits almost no decay after exposure to air at 333 K over 1800 h. Once the temperatures are increased from 293 to 353 K, their PL intensity can be kept as 88.6% of the initial value, much higher than that without the TDPA ligand (i.e., 42.4%). Moreover, their PL QY can be maintained above 50% over 1560 h (65 days) under harsh working conditions of 333 K and 90% humidity. As a proof of concept, the as-assembled white light-emitting diodes display a large color gamut of 125% National Television System Committee standard, suggesting their promising applications in backlight devices.

## INTRODUCTION

Lead-halide perovskite nanocrystals (PNCs), with the formula $APbX_3$ (A = MA (methylammonium), FA (formamidinium), Cs; X = Cl, Br, I), have recently achieved tremendous success in a variety of applications covering solar cells,[1-3] lasers,[4-6] and light-emitting diodes (LEDs) [7-9] due to their excellent photoelectric characteristics such as low formation energy,[10] high photoluminescence quantum yield (PL QY),[11] adjustable emission peak position,[12] and narrow emission full width at half-maximum (fwhm).[13] In particular, the $MAPbBr_3$ PNCs exhibit the strongest structural stability in the lead-halide perovskite family, where the tolerance factor is close to 1. The system has a narrow pure green emission that is centered at the green coordinates required by National Television System Committee (NTSC) or Rec.2020 standards (530~540 nm) and features unique advantages in display applications.[10, 14, 15]

Nevertheless, the intrinsic instability of PNCs against high temperatures and high humidity still remains as a barrier to their use in a variety of optoelectronic devices,[8] and the desorption of surface ligands plays an important role on the degradation of the optical properties of PNCs', as an essential characteristics of ionic crystals of perovskite materials.[16-18] As reported, the most traditional surface ligands of oleic acid and

oleylamine are believed to be bound to the Pb and Br ions on the surface of PNCs through electrostatic interactions or hydrogen bonding, respectively.[19] Those weak binding bond are highly susceptible to breakage at high temperature and high humidity.[20, 21] In this regard, Li *et al*.[22] used the lone pair of non-bonded electrons in alkylammonium salt-type ligand didodecyldimethylammonium bromide to form strong covalent bonds with unoccupied Br ions on the surface of $CsPbBr_3$ NCs, displaying somewhat enhanced thermal stability compared to the as-modified PNCs, which maintained 52% of the initial PL intensity after heated to 333 K for 80 min.[22] To further enhance the carboxylate binds to the undercoordinated Pb ions, perfluorodecanoic acid that has highly electron-withdrawing fluorine atoms was used.[23] This stronger covalent bond significantly improved the thermal stability of the modified $CsPbBr_3$ NCs and maintained 92.1% of the initial intensity of PL after heating at 373 K for 4 h.[23] However, these PNCs still do not satisfy the thermal stability standards for commercial applications. A further improvement of the hydrothermal stability requires the combination of the Lewis acid-base theory to further strengthen the covalent bonds between the ligands and undercoordinated lead ions; a soft Lewis acid.[24, 25] Among the several soft Lewis base ligands, hexylphosphonate was confirmed to be the strongest compared to other bases such as benzoate and difluoro acetate via *ab initio* calculations.[26] In addition, among the different methods for preparing the PNCs, the in-situ growth of PNCs in a polymers stands out as the most promising route for meeting the requirement of display applications as a result of its good film formability with an even surface, ease of fabrication at low cost, and enhanced stability of the PNCs by the wrapping of the polymeric matrix.[27-29] Given the above considerations, the ability to combine polymer encapsulation and strong ligand binding with the suitable hard-soft match for in-situ grown PNCs is expected to be a promising strategy to improve the stability of PNCs. However, this has yet to be in detail to date, due to the complex control of the crystallization processes of PNCs in a polymer compared to colloidal PNCs and thus needs deeper exploration.

In this study, we report on the in-situ growth of $MAPbBr_3$ PNCs@ polyvinylidene fluoride (PVDF) composite films utilizing the knife coating approach, which have excellent optical quality with high hygrothermal stability. Scheme 1 shows the overall synthesis procedure. With the application of the strong coordinated soft Lewis base-tetradecylphosphonic acid (TDPA) as the strong covalent bonds surface ligand, the $MAPbBr_3$ PNCs@PVDF composite film yields a high PL QY of 87.9% with significantly improved high-temperature stability due to the suppressed desorption of ligands. Its PL QY is virtually unchanged after 1800 h of storage at 333 K and over 50% of the initial PL QY is maintained after 65 days at 333 K and at a 90% humidity. With color coordinates of (0.33, 0.33) and a color gamut (125% NTSC standard), the prepared white LED (WLED) exhibits good luminescence performance, opening the door to the use of $MAPbBr_3$ PNCs@PVDF film for backlight liquid crystal devic.

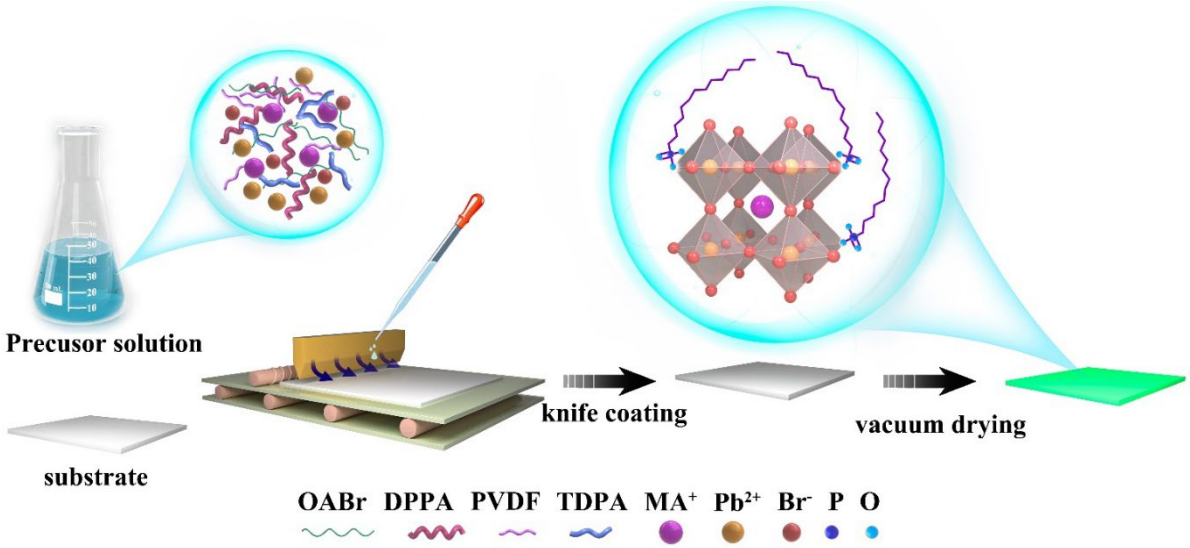


**Scheme 1.** Illustration of the in-situ fabrication of $MAPbBr_3$ perovskite nanocrystals (PNCs) embedded in a PVDF polymer film.

## RESULTS AND DISCUSSION

Scheme 1 shows the preparation procedure of the $MAPbBr_3$ PNCs@PVDF films with various concentrations of TDPA; see details in the Experimental Section. Digital photographs and SEM images of the as-prepared $MAPbBr_3$ PNCs@PVDF films are shown in Figure S1. The films exhibit a stronger green emission under UV irradiation

after adding a certain amount of TDPA, see Figure S1a$_2$-d$_2$, indicating an improved PL QY.[30] The distributions of $MAPbBr_3$ PNCs within the PVDF polymer films are relatively uniform, as revealed by the SEM images in Figure S1a$_3$-d$_3$. Owing to the small size of the $MAPbBr_3$ PNCs, both TEM and HRTEM were employed to clarify the effect of TDPA ligand on the crystal microstructure and size distribution of the as-grown PNCs. Figure 1a,c shows TEM images of the $MAPbBr_3$ PNCs@PVDF films prepared without (as a control) and with 0.03 mmol/mL of TDPA, respectively. Relative to the control sample, it is evident that the TDPA ligand-modified $MAPbBr_3$ PNCs are more uniformly dispersed within the PVDF polymer. A similar phenomenon was also found by Kim *et al*.,[31] were TDPA can significantly reduce agglomeration of the ceramic nanoparticles in the (P(VDF-TrFE)) matrix. As shown in Figure 1b,d, the $MAPbBr_3$ PNCs of both samples are in the form of microspheres, where the interplanar spacing of 0.264 nm and 0.294 nm correspond to the (210) and (200)[15, 32, 33] planes of $MAPbBr_3$, respectively, meaning the successful growth of $MAPbBr_3$ PNCs in a PVDF polymer with high crystallinity.[34] Figure S2 shows the size distributions of $MAPbBr_3$ PNCs in the PVDF films with and without TDPA ligand (statistical base 50), it is surprising that the average crystal size of $MAPbBr_3$ PNCs increased from 6.19 nm to 9.71 nm after modification of TDPA ligand, which is a unified law that the size of $MAPbBr_3$ PNCs slightly increases with the increasing TDPA content. The high concentration of long alkyl chains makes TDPA ligands less nimble and able to coordinate on the PNC surface,[34] thereby extending the period for the crystalline seed to grow and increase the PNC size. Figure S3b-f shows energy dispersive X-ray (EDX) mapping images of C, N, Pb, Br, and P elements, which coincides with that of the PNCs in the TEM image in Figure S3a, suggesting that the TDPA ligand is uniformly distributed on the surface of PNCs.

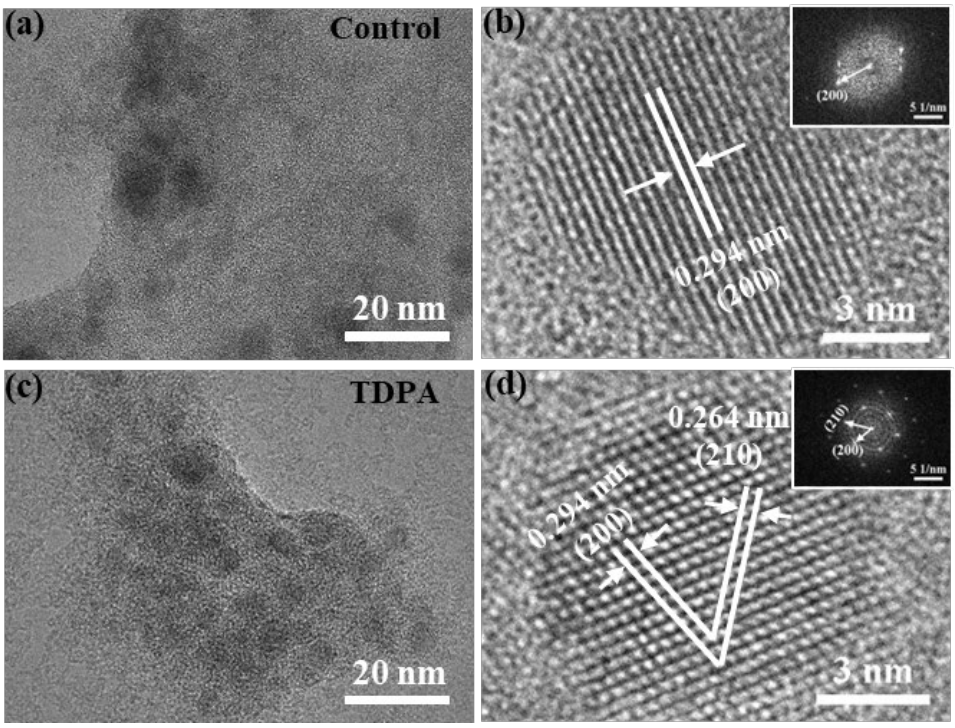


**Figure 1.** The typical TEM (a, c), HRTEM and FFT pattern (inset) of an individual PNC (b, d) from the control (a, b) and 0.03 mmol/mL TDPA-modified (c, d) $MAPbBr_3$ PNCs@PVDF films, respectively.

Figure 2a shows the XRD patterns of the control and TDPA-modified PNCs@polymer films; see Figure S4. Diffraction peaks at 14.9 °, 30.2 °, and 33.7 ° are found in all samples, corresponding to the (100), (200), and (210) planes of cubic-phase $MAPbBr_3$; this further confirms the successful growth of $MAPbBr_3$ PNCs in the PVDF polymer with high crystallinity.[32, 35, 36] The broad diffraction peaks at 20.7 ° are ascribed to the superposition of the amorphous *β*-phase of PVDF[37] and the (110) crystal plane of $MAPbBr_3$.[32] XPS measurements were carried out to confirm the mode of binding between the TDPA and surface of the PNCs. As expected, the P 2*p* and O 1*s* peaks were found in the XPS spectra of the TDPA-modified PNCs@polymer films, Figure 2b,c, means the successful combining of TDPA in the film. In order to confirm the effective binding between the TDPA and the surface of the PNCs, another control film of TDPA@polymer, which was prepared without any perovskite precursor and examined via XPS. The O 1*s* spectrum of the TDPA-free PNC@polymer shows the main oxygen

peak from the P-OH group at 532.95 eV and the P=O group at 531.4 eV in a ratio of 1.8:1 (~ 2:1). This is consistent with previously reported O 1*s* spectra of phosphonic acid derivatives, Figure 2c, and the low interaction between the TDPA and the polymer.[38-40] In contrast, a new peak around 530.75 eV appeared in the O 1*s* spectrum of the TDPA-modified PNCs@polymer films, Figure 2c, which can be ascribed to the formation of a new Pb-O-P covalent bond during adsorption of phosphonate onto a metallic surface, which replaces the bromide vacancy site.[38, 40] Compared with the control sample without TDPA ligand, both binding energies of Pb *4f* and Br *3d* shifted towards lower energy after TDPA modification, see Figure 2d,e; this indicates the effective coordination between the TDPA ligand and the PNCs (Figure S5). The shift can be attributed to the donation of electrons from TDPA to the empty 6*p* orbital of $Pb^{2+}$ and a reduction of the cationic charge on the Pb ion after the binding of P-O- to $Pb^{2+}$.[41-43] Simultaneously, the disturbance of the formed Lewis adduct[44] leads to a change in the static interaction between $Pb^{2+}$ and $Br^-$ ions, and thus lowering the binding energy of Br 3*d*.[41, 42, 45]

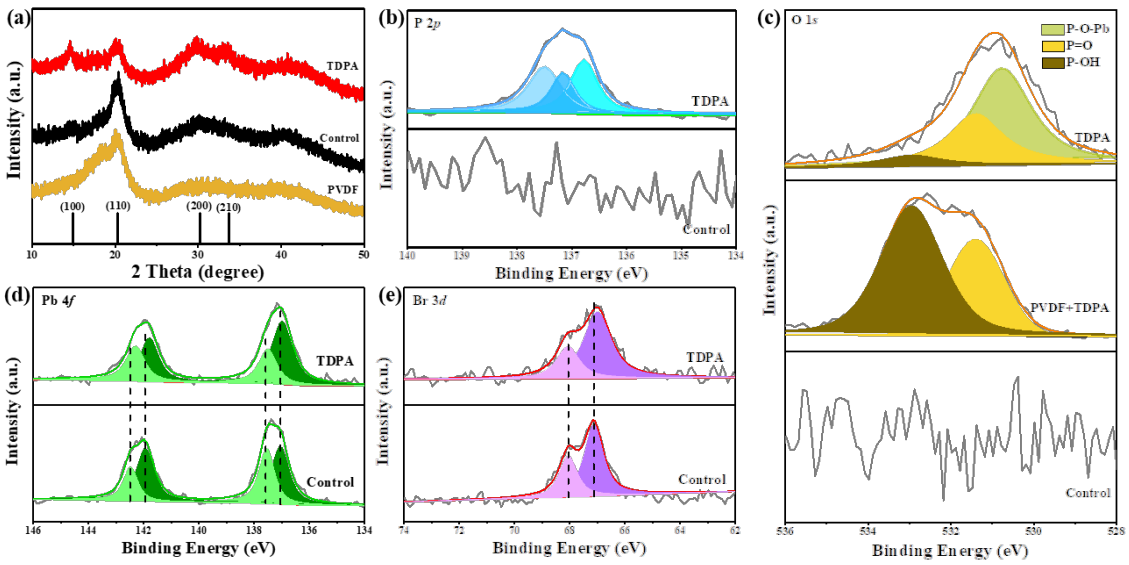


**Figure 2.** XRD patterns (a) of control and TDPA-modified $MAPbBr_3$ PNCs@PVDF and pure PVDF films; XPS spectra of P *2p* (b), O 1*s* (c), Pb *4f* (d) and Br *3d* (e) of TDPA-modified (0.03 mmol/mL) and control $MAPbBr_3$ PNCs@PVDF films.

In Figure 3a, we show the absorption and PL spectra of the control and TDPA-modified $MAPbBr_3$ PNCs@PVDF films synthesized with various TDPA contents. As shown, the PL spectra were slightly red-shifted with increasing TDPA concentration, which can be attributed to the larger particle size (Figure S2) and reduced quantum confinement.[41, 46, 47] When TDPA was added, the PL QY increased from 68.39% (for the control) to 87.89% for the TDPA-modified $MAPbBr_3$ PNCs@PVDF film at 0.03 mmol/mL; see Figure 3b. Such a dramatic improvement can be due to the strong covalent coordination of the TDPA to the unpaired Pb ions on the surface of the $MAPbBr_3$ PNCs, which ultimately lowers the surface defect state. In addition, the time-resolved PL spectra, see Figure 3c, and average PL lifetimes, see Figure 3d, provide convincing evidence of the decreased defect state in the $MAPbBr_3$ PNCs. The $\tau_{avg}$ of 43.39 ns for 0.03 mmol/mL TDPA-treated films, represents an increase of 1.8 times when compared to the control perovskite film (23.53 ns), demonstrating that the non-radiative trapping in the surface sites of $MAPbBr_3$ PNCs is suppressed; the time constants and the normalized amplitudes of the components obtained from the triexponential decay fit are detailed in Table S1. When the concentration of TDPA ligand was increased to 0.05 mmol/mL, the PL QY and average lifetime decreased. This was attributed to the fact that the excessive TDPA ligands lead to more surface defects being exposed due to the competing adsorption of different ligands species.[48]

To understand the mechanisms leading to higher PL QY values in the TDPA-modified $MAPbBr_3$ PNCs@PVDF films, as well as to their remarkable exciton recombination dynamics, we performed density functional theory (DFT)[49] calculations; the Supplementary Information, Figure S6 provides further details on the models. The negative value (-1.248 eV, Figure S7) for the formation energy of $MAPbBr_3$ containing bromine vacancies ($V_{Br}$) (showing bare Pb ions on the surface) indicates that the $V_{Br}$ will spontaneously generate on the surface of $MAPbBr_3$, which agrees with the literature[50-52] and experimental results (see Figure 3c,d). However, after adsorption of TDPA, the more negative formation energy (-1.425 eV) of $MAPbBr_3$-$V_{Br}$ indicates an enhanced stability, owing to the passivation of TDPA on the dangling bond of the bare

Pb ions. Therefore, the modification of the TDPA can improve the structural stability of $MAPbBr_3$ crystals.[53] To further elucidate the reason for the enhanced optical properties, the adsorption energy of TDPA on the $MAPbBr_3$ surface was also calculated, and details of the calculation and underlyng equations are presented in the Supporting Information. As shown in Figure S7, the adsorption energy of TDPA on the $MAPbBr_3$ crystal surface is -7.607 eV, which absolute value is higher than 0.1-0.42 eV,[54] indicating that the adsorption between TDPA and $MAPbBr_3$ is chemisorption rather than the physisorption, namely the strong binding of the Pb-O bonds,[55, 56] which results in the improved optical properties of $MAPbBr_3$ PNCs. As seen in Figure 3e,f, the conduction band of $MAPbBr_3$ is mainly contributed by the Pb-*p* orbital, while the valence band is mainly contributed by the Br-*p* orbital. When a Br vacancy defect exists on the surface of $MAPbBr_3$, the Pb-Br bond breaks, causing the appearance of unpaired electrons around Pb, with the existence of dangling bonds around Pb (*i.e.*, Pb defect states of *p* orbital), [53, 57, 58] and a conduction band with a high concentration of defective Pb-*p* states near the Fermi energy level (marked by the dashed box, Figure 3f). Once the Br vacancies are passivated by TDPA, Figure 3g,h, TDPA bonds with Pb and can inhibit the formation of Br vacancies on the surface of $MAPbBr_3$, leading to the disappearance of the defect states near the Fermi energy level.[58, 59] Consequently, the surface modification due to the strong covalent bonds of TDPA can attenuate the defect-induced non-radiative recombination rate, resulting in the enhancement of $MAPbBr_3$ luminescence performance.

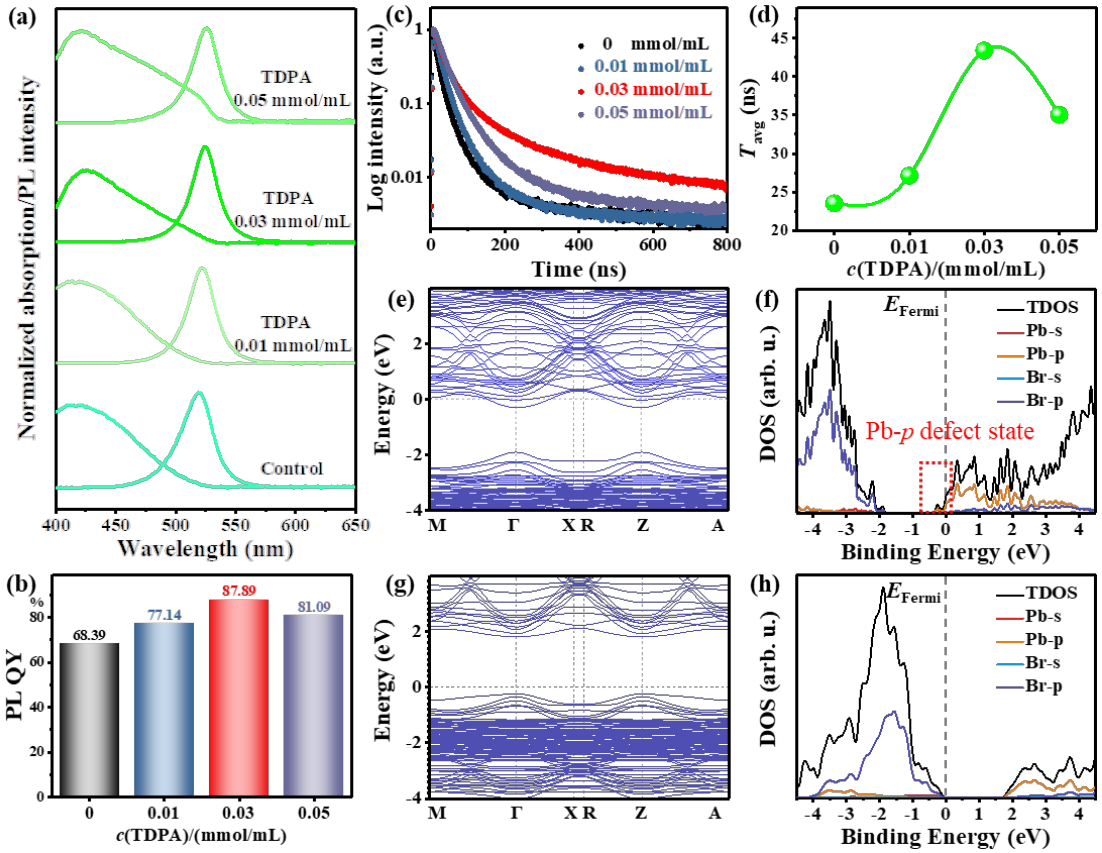


**Figure 3.** Normalized absorption/PL spectra (a), PL QYs (b), time-resolved PL decay curves (c), and the average decay lifetimes (d) of $MAPbBr_3$ PNCs@PVDF films prepared with various TDPA contents; electronic energy band structure (e, g) and density of states (f, h) of the $MAPbBr_3$ slab with Br vacancies (e and f) and TDPA ligand (g and h).

In addition to enhancing the emission efficiency, the TDPA treatment has a profound effect on the thermal stability of the as-prepared $MAPbBr_3$ PNCs@PVDF film. Figure 4a shows the PL QY of the TDPA-treated film, which retains near unity PL QY after exposing under 333 K for 1800 h, while some decrease is observed in the control sample, with a significant red shift in its peak position; see Figure S8. The red shift is mostly due to the high temperature-induced Ostwald ripening between adjacent PNCs within the film that results in an increase in PNCs size with more defects.[60] An undetectable spectra shift was observed in the optimized sample, and this indicates the suppressed regrowth of the adjacent PNCs within the film due to the enhanced adhesion

between the $MAPbBr_3$ PNCs and the PVDF polymer by the TDPA ligand.[28, 31] We monitored the PL of $MAPbBr_3$ PNCs@PVDF film in situ as it was heated from T = 293 to 353 K (with a heating rate 3 $K \cdot min^{-1}$) to explore the PL thermal quenching behavior. The PL intensity of the control film decreases noticeably as the test temperature rises, with only 42.35% of the initial intensity remaining when the temperature was raised to 353 K, as can be observed in Figure 4b. In agreement with previous reports,[18, 61, 62] the increase in temperature intensified the lattice vibrations of the PNCs inside the film, thereby breaking the weak binding bonds between the surface of the PNCs and ligands and increasing the surface defect states,[63] thereby inducing an electro-acoustic coupling and improving the non-radiative composite.[64] Strikingly, the addition of TDPA increased the thermal resistance of the PNCs, Figure 4c, leading to a high PL strength (maintaining 88.55% of the initial), which improved the performance compared to the control sample. As demonstrated in Figure S9 and Table S2, a similar result was reached by examining the time-resolved PL spectra of the $MAPbBr_3$ PNCs@PVDF films before and after their variable-temperature thermal treatment process. The average lifetime determined by the tri-exponential decay of the control samples dramatically decreased after heat treatment; this is typically as a result of accelerated ligand desorption from the PNC surface and partial PNC decomposition,[65] resulting in an increased defect density in the $MAPbBr_3$ PNCs and poor performance. There a lower shift in the decay curve of the $MAPbBr_3$ PNCs@PVDF film that was treated with TDPA ligand, and the average lifetime was alomst unaltered. This result suggests that the TDPA ligand inhibits the desorption of the ligand by strengthening the spatial confinement of PVDF polymer and the strong binding P-O-Pb link between the ligand and the PNCs, thereby suppressing the nonradiative complexation of the PNCs induced by lattice vibrations.[40] The remarkable thermal stability caused by the TDPA ligand was also a result of the significant proportion of organic materials carried by its lengthy alkyl chain.[66]

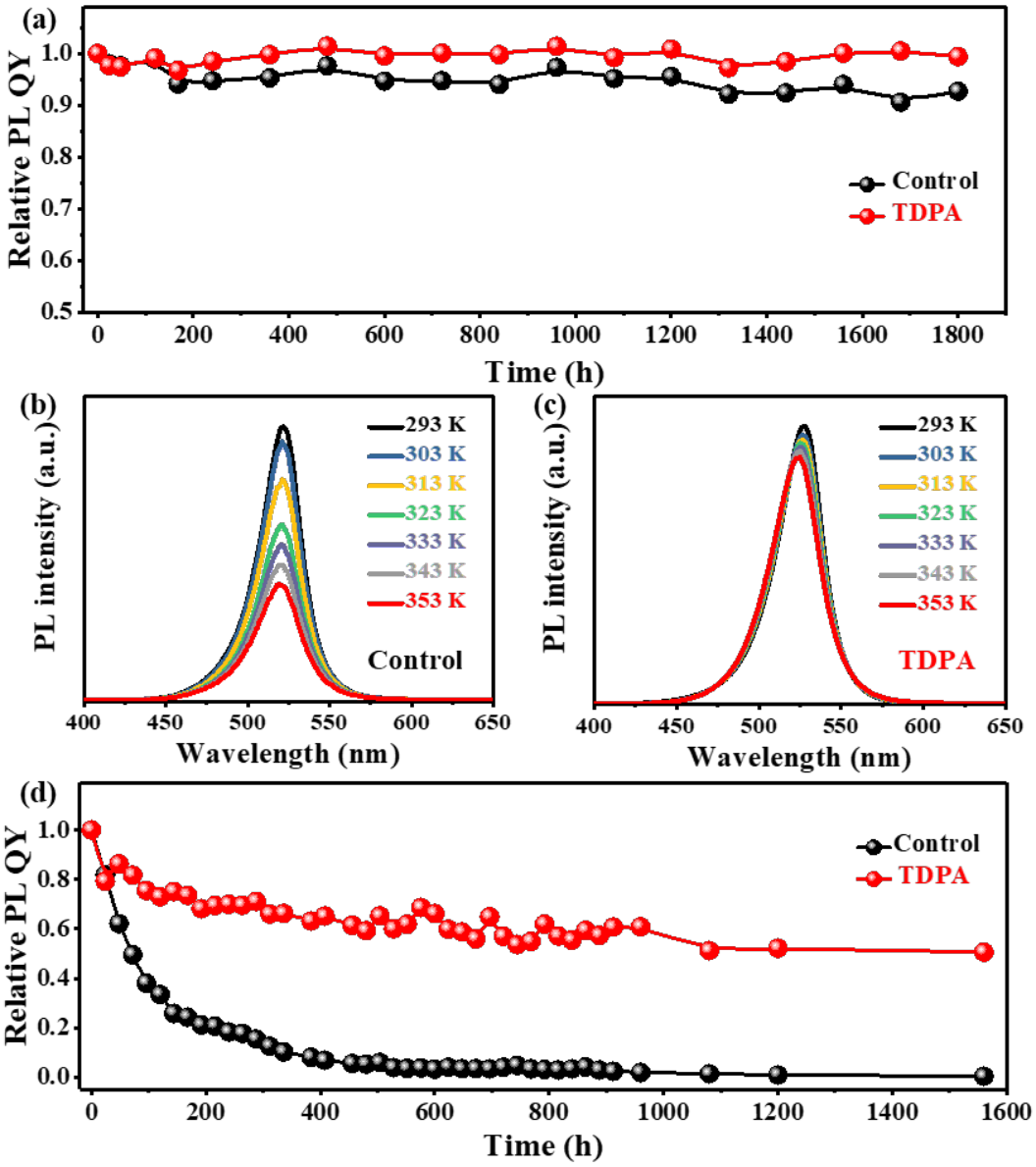


**Figure 4.** Relative PL QY versus exposing time under 333 K treated (a), PL intensity versus temperature (b, c), and relative PL QY versus exposing time under 333 K and 90% humidity (d) of control and TDPA-modified $MAPbBr_3$ PNCs@PVDF films.

In order to test their hydrothermal stability, the control and optimized samples were stored in a 373 K thermostat with a constant humidity of 90% for up to 1580 h and the PL intensities were monitored periodically. Figure 4d shows the remnant PL integrated intensities of both samples treated in the thermostat at a different time (where the initial PL integrated intensity is 100%). The PL of the control sample completely vanished after 600 h, even when encapsulated by PVDF with DPPA and OABr ligands

protection. Notably, the optimized sample maintains a high stability at 333 K and 90% humidity, and its PL QY gradually stabilizes after 1560 h and is able to maintain 51% of the initial efficiency. Furthermore, after being immersed in water for 240 h at room temperature, the TDPA-modified film's fluorescence intensity remained unchanged under a 365 nm UV lamp irradiation, while the intensity of the control film significantly decreased (Figure S10). It is known that the strong spatial site resistance of TDPA reduces the opportunity for water molecules to contact the surface of $MAPbBr_3$ PNCs, which contributes to an improved water stability.[40] The results verify that the optimized film exhibits superior hygrothermal stability, which is believed to be a result of the powerful TDPA modification. This performance is comparable to the optimal properties reported in the literature to date; see Table S3.

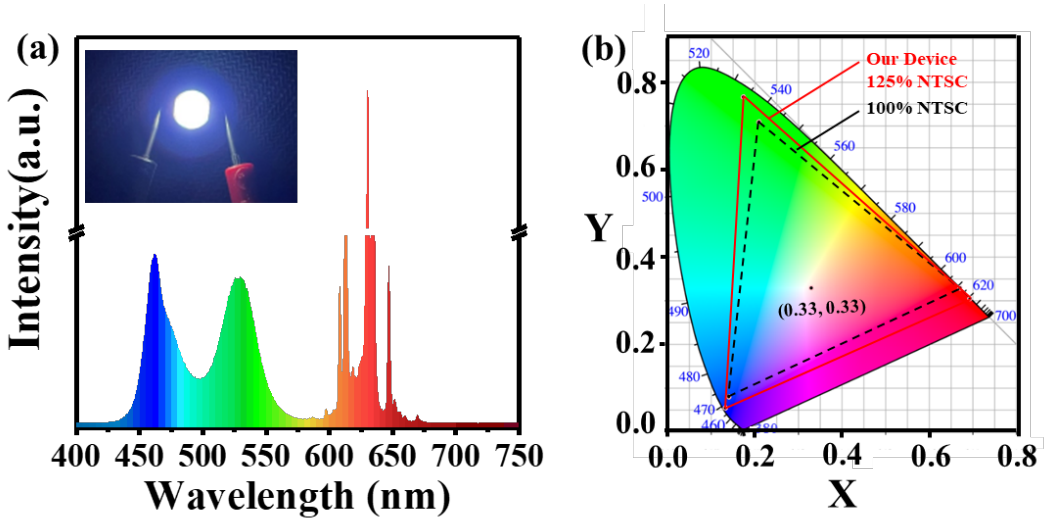


**Figure 5.** The spectrum of the WLED (inset: the photograph of the device operated at 2.5 V) (a), the CIE color coordinate (black point) and the color triangle (red line) compared to the 100% NTSC standard (back line) of the as-fabricated WLED device (b).

With significantly improved PL QY and high stability, the TDPA-modified $MAPbBr_3$ PNCs@PVDF film has potential applicability in white light emitting diodes (WLED) devices. Figure 5a shows the spectrum of the WLED fabricated by encapsulating green emissive $MAPbBr_3$@PVDF film and red commercial $K_2SiF_6:Mn^{4+}$ phosphor on a blue-emitting chip (460 nm) with an input voltage of 2.5 V. And the top

left inset in Figure 5a is a digital photo of the optimized device under the operation of 2.5 V, which emits natural white light with the luminous efficiency of 31 lm· $W^{-1}$. The commission international de l'Eclairage (CIE) coordinate of the WLED can be adjusted to (0.33, 0.33) with correlated color temperature (CCT) of 5554 K, which is equal to the standard white color, as shown in Figure 5b. The corresponding triangle (red line) covers 125% of NTSC standard color (black line), which represents a signficiant potential of the TDPA-modified $MAPbBr_3$ PNCs@PVDF film in lighting and display applications.

## CONCLUSIONS

In summary, we have demonstrated that the preferred TDPA as the soft Lewis ligand could significantly enhance the optical properties and hygrothermal stability of $MAPbBr_3$ organic-inorganic PNCs, which are in-situ grown within PVDF film in a controlled manner. The introduced TDPA ligand facilitates the formation of strong covalent coordinated P-O-Pb bond, which could not only make efficient passivation of the surface defects of PNCs, but also enable the remarkably suppressed desorption of the ligand from the surface of PNCs under high-temperature environments. The as-fabricated $MAPbBr_3$-PNCs@PVDF film exhibits an excellent optical performance with a narrow FWHM (28.7 nm) and high PL QY (87.9%). Furthermore, the PL QY is highly stable with nearly no decay once exposed in air at 333 K over 1800 h. Additionally, their PL peak intensity could be maintained at 88.6% of its initial value when the temperature is increased from 293 to 353 K, much higher than that without TDPA ligand (i.e., 42.4%). Moreover, their PL QY could be maintained more than 50% over 1560 h (65 days) under harsh working conditions of 333 K and 90% humidity. Finally, the WLEDs based on $MAPbBr_3$ PNCs@PVDF film has been developed, which deliver a large color gamut of 125% NTSC standard with color coordinates at (0.33, 0.33). The present work might give some insight on fabricating organic-inorganic perovskite materials with profoundly enhanced hydrothermal stability, to push forward their applications in backlight devices.

## EXPERIMENTAL SECTION

*Materials*: Methylammonium bromide (MABr, 99.5%, Xi'an Polymer Light Technology Co., China), Lead (II) bromide ($PbBr_2$, 99%, Aladdin), n-Octylamine hydrobromide (OABr, 99.5%, Xi'an Polymer Light Technology Co., China), 3,3-Diphenylpropylamine (DPPA, 97%, Macklin), Tetradecylphosphonic acid (TDPA, ＞ 98%, Aladdin), N, N-Dimethylformamide (DMF, 99.9%, Aladdin) and polyvinylidene fluoride (PVDF, $M_W \approx$ 780,000, Solvay). All chemicals were directly used as received without further experimental treatment.

*Preparation of precursor solution*: For preparing the precursor solution, it was modified from the previously reported approach.[67] In a typical procedure, 124.08 mg (1.1 mmol) of MABr, 508.88 mg (1.4 mmol) of $PbBr_2$, 7.4 g of PVDF, and 80 mL of DMF were mixed into a 100 mL Erlenmeyer flask and mechanically stirred for 12 h at room temperature to completely dissolve and mix the precursors. Subsequently, 175.81 mg (0.83 mmol) of DPPA and 14.57 mg (0.07 mmol) of OABr were added to an Erlenmeyer flask followed by 2 h stirring. Target TDPA concentrations (0, 0.01, 0.03, and 0.05 mmol/mL) were added to the 10 mL of the aforementioned solution using a pipette, and the mixture was stirred for 2 hours before use.

*Preparation of $MAPbBr_3$ PNCs@PVDF films*: $MAPbBr_3$ PNCs@PVDF films were fabricated by a knife coating method, and a flat glass was selected as the substrate. The above-mentioned precursor solution was first transferred to one end of the glass substrate and spread the precursor evenly with a coater. Then the glass plate was transferred into a vacuum drying oven at 353 K immediately, and maintained at a low pressure for 5 min until the precursor on the glass solidified into a film and turns green. The preparation process is shown in Scheme 1.

*Fabrication of WLED devices*: Firstly, red commercial $K_2SiF_6:Mn^{4+}$ phosphor was encapsulated into UV cure adhesive, followed by a UV curing process for ~2 h to form the red emissive layer, which was directly laid onto a blue light LED chip (460 nm).

Then, the optimized $MAPbBr_3$ PNCs@PVDF film was placed on top of the red emissive layer.

*Characterization*: The structure and morphology of as-prepared $MAPbBr_3$ PNCs@PVDF films were analyzed using field emission scanning electron microscopy (SEM, S-4800, Hitachi, Japan), high-resolution transmission electron microscopy (HRTEM, JEM-2100F, JEOL, Japan), and X-ray diffraction (XRD, D8 Advance, Bruker, Germany). The surface species and chemical states of the PNCs were measured by X-ray photoelectron spectroscopy (XPS, ESCALAB 250Xi, Thermo Fisher Scientific, USA). The PL spectra, absolute PL QY, decay curves, and in-suit variable-temperature test of the films were measured using a fluorescence spectrometer (Fluromax-4P, Horiba Jobin Yvon, France) equipped with a quantum-yield accessory, a time-correlated single photon-counting spectrometer, and a Lakeshore 331 temperature controller. A Nano LED (wavelength: 370 nm) was utilized as the exciting source for PL decay measurements. The UV-vis measurements were performed on a UV-vis scanning spectrophotometer (U-3900, Hitachi, Japan). Electroluminescence (EL) spectra of WLEDs were measured on a spectrometer (Maya 2000Pro, Ocean Insight, USA).

*Density functional theory (DFT) computation*: To clarify the improvement mechanism of TDPA ligands on the optical properties of $MAPbBr_3$ PNCs, the electronic structure properties, the perovskite formation energy, and ligand surface adsorption energy of $MAPbBr_3$ perovskite were calculated based on density functional theory (DFT). The Vienna Ab-initio Simulation Package (VASP) software package was used as the computational software,[68] while the Perdew-Burke-Ernzerhof (PBE) functional of the generalized gradient approximation (GGA) was chosen for the exchange-correlation generalization function.[69] The electron-ion interaction was described by the projector-augmented wave (PAW) potentials with a cutoff energy of 400 eV confirmed by the convergence test. The valence electron configurations of Pb, Br, C, N, O, P, and H were $6s^26p^2$, $4s^24p^5$, $2s^22p^2$, $2s^22p^3$, $2s^22p^4$, $3s^23p^3$, and $1s^1$, respectively. The self-consistent convergence accuracy of the structure optimization

was $1.0\times10^{-4}$ eV for the energy, and the convergence accuracy of the force was 0.05 eV/Å.

## ASSOCIATED CONTENT

### Supporting Information

SEM images, TEM, structural characterizations, XPS spectra, optical performances, and calculation of DFT of as-fabricated samples (PDF).

## AUTHOR INFORMATION


### Corresponding Author

* E-mail: zhengzhao2007@163.com (J. Zheng)

* E-mail: weiyouyang@tsinghua.org.cn (W. Yang)


### Author Contributions

The manuscript was written through the contributions of all authors. All authors have given approval to the final version of the manuscript. Hui Fu, Jinju Zheng and Weiyou Yang played the leading role, other authors contributed equally.

### Notes

The authors declare no competing financial interest.

## ACKNOWLEDGMENT


This work was supported by Scientific Research Fund of Zhejiang Provincial Education Department (Grant No. Y202250313), Scientific Research Project Funded by Ningbo University of Technology (Grant No. 2022KQ11), Cultivation Project

Funded by Ningbo University of Technology (Grant No. 2022TS26), "Science and Technology Innovation 2025" of Ningbo Foundation (Grant No. 2020Z061), National Natural Science Foundation of China (NSFC, Grant No. 62205165).

## REFERENCES

(1) Tian, J.; Xue, Q.; Yao, Q.; Li, N.; Brabec, C. J.; Yip, H. L. Inorganic halide perovskite solar cells: Progress and challenges. *Adv. Energy. Mater.* **2020,** 10 (23), 2000183, DOI: 10.1002/aenm.202000183.
(2) Tian, J.; Wang, J.; Xue, Q.; Niu, T.; Yan, L.; Zhu, Z.; Li, N.; Brabec, C. J.; Yip, H. L.; Cao, Y. Composition engineering of all-inorganic perovskite film for efficient and operationally stable solar cells. *Adv. Funct. Mater.* **2020,** 30 (28), 2001764, DOI: 10.1002/adfm.202001764.
(3) Lee, S.; Moon, J.; Ryu, J.; Parida, B.; Yoon, S.; Lee, D.-G.; Cho, J. S.; Hayase, S.; Kang, D.-W. Inorganic narrow bandgap $CsPb_{0.4}Sn_{0.6}I_{2.4}Br_{0.6}$ perovskite solar cells with exceptional efficiency. *Nano Energy* **2020,** 77, 105309, DOI: 10.1016/j.nanoen.2020.105309.
(4) Dong, H.; Zhang, C.; Liu, X.; Yao, J.; Zhao, Y. S. Materials chemistry and engineering in metal halide perovskite lasers. *Chem. Soc. Rev.* **2020,** 49 (3), 951-982, DOI: 10.1039/c9cs00598f.
(5) Huang, L.; Gao, Q.; Sun, L. D.; Dong, H.; Shi, S.; Cai, T.; Liao, Q.; Yan, C. H. Composition-graded cesium lead halide perovskite nanowires with tunable dual-color lasing performance. *Adv. Mater.* **2018,** 30 (27), e1800596, DOI: 10.1002/adma.201800596.
(6) Zhang, Q.; Su, R.; Liu, X.; Xing, J.; Sum, T. C.; Xiong, Q. High-quality whispering-gallery-mode lasing from cesium lead halide perovskite nanoplatelets. *Adv. Funct. Mater.* **2016,** 26 (34), 6238-6245, DOI: 10.1002/adfm.201601690.
(7) Wang, Y.; Wang, S.; Yoo, J.; Yoon, D.; Li, T.; Wang, Y. Methylammonium cation-regulated controllable preparation of $CsPbBr_3$ perovskite quantum dots in polystyrene fiber with enhanced water and UV light stabilities. *Inorg. Chem.* **2023,** 62 (22), 8626-8634, DOI: 10.1021/acs.inorgchem.3c00702.
(8) Yang, C.; Niu, W.; Chen, R.; Pang, T.; Lin, J.; Zheng, Y.; Zhang, R.; Wang, Z.; Huang, P.; Huang, F.; Chen, D. In situ growth of ultrapure green-emitting $FAPbBr_3$-PVDF films via a synergetic dual-additive strategy for wide color gamut backlit display. *Adv. Mater. Technol-US.* **2022,** 7 (8), 2200100, DOI: 10.1002/admt.202200100.
(9) Shen, W.; Yang, L.; Feng, J.; Chen, Y.; Wang, W.; Zhang, J.; Liu, L.; Cao, K.; Chen, S. Environmentally friendly syntheses of self-healed and printable $CsPbBr_3$ nanocrystals. *Inorg. Chem.* **2022,** 61 (23), 8604-8610, DOI: 10.1021/acs.inorgchem.2c01113.
(10) Zhang, F.; Zhong, H.; Chen, C.; Wu, X. G.; Hu, X.; Huang, H.; Han, J.; Zou, B.; Dong, Y. Brightly luminescent and color-tunable colloidal $CH_3NH_3PbX_3$ (X = Br, I,

Cl) quantum dots potential alternatives for display technology. *ACS nano* **2015,** 9 (4), 4533-42, DOI: 10.1021/acsnano.5b01154.
(11) Bao, X.; Li, M.; Zhao, J.; Xia, Z. The postsynthetic anion exchange of $CsPbI_3$ nanocrystals for photoluminescence tuning and enhanced quantum efficiency. *J. Mater. Chem. C* **2020,** 8, 12302-12307, DOI: 10.1039/d0tc03023f.
(12) Dey, A.; Ye, J.; De, A.; Debroye, E.; Ha, S. K.; Bladt, E.; Kshirsagar, A. S.; Wang, Z.; Yin, J.; Wang, Y.; Quan, L. N.; Yan, F.; Gao, M.; Li, X.; Shamsi, J.; Debnath, T.; Cao, M.; Scheel, M. A.; Kumar, S.; Steele, J. A.; Gerhard, M.; Chouhan, L.; Xu, K.; Wu, X. G.; Li, Y.; Zhang, Y.; Dutta, A.; Han, C.; Vincon, I.; Rogach, A. L.; Nag, A.; Samanta, A.; Korgel, B. A.; Shih, C. J.; Gamelin, D. R.; Son, D. H.; Zeng, H.; Zhong, H.; Sun, H.; Demir, H. V.; Scheblykin, I. G.; Mora-Sero, I.; Stolarczyk, J. K.; Zhang, J. Z.; Feldmann, J.; Hofkens, J.; Luther, J. M.; Perez-Prieto, J.; Li, L.; Manna, L.; Bodnarchuk, M. I.; Kovalenko, M. V.; Roeffaers, M. B. J.; Pradhan, N.; Mohammed, O. F.; Bakr, O. M.; Yang, P.; Muller-Buschbaum, P.; Kamat, P. V.; Bao, Q.; Zhang, Q.; Krahne, R.; Galian, R. E.; Stranks, S. D.; Bals, S.; Biju, V.; Tisdale, W. A.; Yan, Y.; Hoye, R. L. Z.; Polavarapu, L. State of the art and prospects for halide perovskite nanocrystals. *ACS nano* **2021,** 15 (7), 10775-10981, DOI: 10.1021/acsnano.0c08903.
(13) Wang, X.; Bao, Z.; Chang, Y.-C.; Liu, R.-S. Perovskite quantum dots for application in high color gamut backlighting display of light-emitting diodes. *ACS Energy Lett.* **2020,** 5 (11), 3374-3396, DOI: 10.1021/acsenergylett.0c01860.
(14) Yan, N.; Yin, H.; Wang, Z.; Yuan, H.; Xin, Y.; Tang, Y. Role of ammonium derivative ligands on optical properties of $CH_3NH_3PbBr_3$ perovskite nanocrystals. *Langmuir* **2019,** 35 (47), 15151-15157, DOI: 10.1021/acs.langmuir.9b02129.
(15) Binbin, L.; Ying-Chih, P.; A., L. S.; Yi, Y.; Liqiang, L.; Yat, L.; Xueming, L.; Z., Z. J. Organolead halide perovskite nanocrystals branched capping ligands control crystal size and stability. *Angew. Chem. Int. Ed.* **2016,** 55 (31), 8864-8868, DOI: 10.1002/anie.201602236.
(16) Diroll, B. T.; Nedelcu, G.; Kovalenko, M. V.; Schaller, R. D. High-temperature photoluminescence of $CsPbX_3$ (X = Cl, Br, I) nanocrystals. *Adv. Funct. Mater.* **2017,** 27 (21), 1606750, DOI: 10.1002/adfm.201606750.
(17) Wang, X.; Lian, X.; Zhang, Z.; Gao, H. Could nanocomposites continue the success of halide perovskites? *ACS Energy Lett.* **2019,** 4 (6), 1446-1454, DOI: 10.1021/acsenergylett.9b00580.
(18) Dang, Z.; Dhanabalan, B.; Castelli, A.; Dhall, R.; Bustillo, K. C.; Marchelli, D.; Spirito, D.; Petralanda, U.; Shamsi, J.; Manna, L.; Krahne, R.; Arciniegas, M. P. Temperature-driven transformation of $CsPbBr_3$ nanoplatelets into mosaic nanotiles in solution through self-assembly. *Nano. Lett.* **2020,** 20 (3), 1808-1818, DOI: 10.1021/acs.nanolett.9b05036.
(19) Roo, J. D.; Ibáñez, M.; Geiregat, P.; Nedelcu, G.; Walravens, W.; Maes, J.; Martins, J. C.; Driessche, I. V.; Kovalenko, M. V.; Hens, Z. Highly dynamic ligand binding and light absorption coefficient of cesium lead bromide perovskite nanocrystals. *ACS nano* **2016,** 10 (2), 2071-2081, DOI: 10.1021/acsnano.5b06295.

(20) Bai, Y.; Hao, M.; Ding, S.; Chen, P.; Wang, L. Surface chemistry engineering of perovskite quantum dots: strategies, applications, and perspectives. *Adv. Mater.* **2022,** 34 (4), e2105958, DOI: 10.1002/adma.202105958.
(21) ten Brinck, S.; Infante, I. Surface termination, morphology, and bright photoluminescence of cesium lead halide perovskite nanocrystals. *ACS Energy Lett.* **2016,** 1 (6), 1266-1272, DOI: 10.1021/acsenergylett.6b00595.
(22) Li, X.; Cai, W.; Guan, H.; Zhao, S.; Cao, S.; Chen, C.; Liu, M.; Zang, Z. Highly stable $CsPbBr_3$ quantum dots by silica-coating and ligand modification for white light-emitting diodes and visible light communication. *Chem. Eng. J.* **2021,** 419, 129551, DOI: 10.1016/j.cej.2021.129551.
(23) Sato, D.; Iso, Y.; Isobe, T. Effective stabilization of perovskite cesium lead bromide nanocrystals through facile surface modification by perfluorocarbon acid. *ACS omega* **2020,** 5 (2), 1178-1187, DOI: 10.1021/acsomega.9b03472.
(24) Boles, M. A.; Ling, D.; Hyeon, T.; Talapin, D. V. The surface science of nanocrystals. *Nat. Mater.* **2016,** 15 (2), 141-53, DOI: 10.1038/nmat4526.
(25) Owen, J. Nanocrystal structure. The coordination chemistry of nanocrystal surfaces. *Science* **2015,** 347 (6222), 615-6, DOI: 10.1126/science.1259924.
(26) Nenon, D. P.; Pressler, K.; Kang, J.; Koscher, B. A.; Olshansky, J. H.; Osowiecki, W. T.; Koc, M. A.; Wang, L. W.; Alivisatos, A. P. Design principles for trap-free $CsPbX_3$ nanocrystals: enumerating and eliminating surface halide vacancies with softer lewis bases. *J. Am. Chem. Soc.* **2018,** 140 (50), 17760-17772, DOI: 10.1021/jacs.8b11035.
(27) Chang, S.; Bai, Z.; Zhong, H. In situ fabricated perovskite nanocrystals: a revolution in optical materials. Adv. Opt. Mater. 2018, 6 (18), 1800380, DOI: 10.1002/adom.201800380.
(28) Zhou, Q.; Bai, Z.; Lu, W.-g.; Wang, Y.; Zou, B.; Zhong, H. In situ fabrication of halide perovskite nanocrystal-embedded polymer composite films with enhanced photoluminescence for display backlights. *Adv. Mater.* **2016,** 28, 9163-9168, DOI: 10.1002/adma.201602651.
(29) Liu, W.; Fu, H.; Liao, H.; Liang, Z.; Ye, Y.; Zheng, J.; Yang, W. In situ synthesis of coaxial $CsPbX_3$@polymer (X = Cl, Br, I) fibers with significantly enhanced water stability. *J. Mater. Chem. C* **2020,** 8 (40), 13972-13975, DOI: 10.1039/d0tc04035e.
(30) Li, Z.; Kong, L.; Huang, S.; Li, L. Highly luminescent and ultrastable $CsPbBr_3$ perovskite quantum dots incorporated into a silica/alumina monolith. *Angew. Chem. Int. Ed.* **2017,** 56 (28), 8134-8138, DOI: 10.1002/anie.201703264.
(31) Kim, S.-R.; Yoo, J.-H.; Kim, J. H.; Cho, Y. S.; Park, J.-W. Mechanical and piezoelectric properties of surface modified $(Na,K)NbO_3$-based nanoparticle-embedded piezoelectric polymer composite nanofibers for flexible piezoelectric nanogenerators. *Nano Energy* **2021,** 79, 105445, DOI: 10.1016/j.nanoen.2020.105445.
(32) Meng, L.; Yang, C.; Meng, J.; Wang, Y.; Ge, Y.; Shao, Z.; Zhang, G.; Rogach, A. L.; Zhong, H. In-situ fabricated anisotropic halide perovskite nanocrystals in polyvinylalcohol nanofibers: Shape tuning and polarized emission. *Nano Res.* **2019,** 12 (6), 1411-1416, DOI: 10.1007/s12274-019-2353-4.

(33) Schmidt, L. C.; Pertegas, A.; Gonzalez-Carrero, S.; Malinkiewicz, O.; Agouram, S.; Minguez Espallargas, G.; Bolink, H. J.; Galian, R. E.; Perez-Prieto, J. Nontemplate synthesis of $CH_3NH_3PbBr_3$ perovskite nanoparticles. *J. Am. Chem. Soc.* **2014,** 136 (3), 850-3, DOI: 10.1021/ja4109209.
(34) Chun, F.; Zhang, B.; Li, Y.; Li, W.; Xie, M.; Peng, X.; Yan, C.; Chen, Z.; Zhang, H.; Yang, W. Internally-externally defects-tailored $MAPbI_3$ perovskites with highly enhanced air stability and quantum yield. *Chem. Eng. J.* **2020**, 125715, DOI: 10.1016/j.cej.2020.125715.
(35) Liu, P.; He, X.; Ren, J.; Liao, Q.; Yao, J.; Fu, H. Organic-inorganic hybrid perovskite nanowire laser arrays. *ACS nano* **2017,** 11 (6), 5766-5773, DOI: 10.1021/acsnano.7b01351.
(36) Lu, W.-G.; Wu, X.-G.; Huang, S.; Wang, L.; Zhou, Q.; Zou, B.; Zhong, H.; Wang, Y. Strong polarized photoluminescence from stretched perovskite-nanocrystal-embedded polymer composite films. *Adv. Opt. Mater.* **2017,** 5 (23), 1700594, DOI: 10.1002/adom.201700594.
(37) Chen, H.; Zhou, L.; Fang, Z.; Wang, S.; Yang, T.; Zhu, L.; Hou, X.; Wang, H.; Wang, Z. L. Piezoelectric nanogenerator based on in situ growth all-inorganic $CsPbBr_3$ perovskite nanocrystals in PVDF fibers with long-term stability. *Adv. Funct. Mater.* **2021,** 31 (19), 2011073, DOI: 10.1002/adfm.202011073.
(38) Kim, J. S.; Heo, J. M.; Park, G. S.; Woo, S. J.; Cho, C.; Yun, H. J.; Kim, D. H.; Park, J.; Lee, S. C.; Park, S. H.; Yoon, E.; Greenham, N. C.; Lee, T. W. Ultra-bright, efficient and stable perovskite light-emitting diodes. *Nature* **2022,** 611 (7937), 688-694, DOI: 10.1038/s41586-022-05304-w.
(39) Ambroz, F.; Xu, W.; Gadipelli, S.; Brett, D. J. L.; Lin, C. T.; Contini, C.; McLachlan, M. A.; Durrant, J. R.; Parkin, I. P.; Macdonald, T. J. Room Temperature synthesis of phosphine-capped lead bromide perovskite nanocrystals without coordinating solvents. *Part. Part. Syst. Char.* **2019,** 37 (1), 1900391, DOI: 10.1002/ppsc.201900391.
(40) Xuan, T.; Yang, X.; Lou, S.; Huang, J.; Liu, Y.; Yu, J.; Li, H.; Wong, K. L.; Wang, C.; Wang, J. Highly stable $CsPbBr_3$ quantum dots coated with alkyl phosphate for white light-emitting diodes. *Nanoscale* **2017,** 9 (40), 15286-15290, DOI: 10.1039/c7nr04179a.
(41) Kong, L.; Zhang, X.; Li, Y.; Wang, H.; Jiang, Y.; Wang, S.; You, M.; Zhang, C.; Zhang, T.; Kershaw, S. V.; Zheng, W.; Yang, Y.; Lin, Q.; Yuan, M.; Rogach, A. L.; Yang, X. Smoothing the energy transfer pathway in quasi-2D perovskite films using methanesulfonate leads to highly efficient light-emitting devices. *Nat. Commun.* **2021,** 12 (1), 1246, DOI: 10.1038/s41467-021-21522-8.
(42) Ma, D.; Lin, K.; Dong, Y.; Choubisa, H.; Proppe, A. H.; Wu, D.; Wang, Y. K.; Chen, B.; Li, P.; Fan, J. Z.; Yuan, F.; Johnston, A.; Liu, Y.; Kang, Y.; Lu, Z. H.; Wei, Z.; Sargent, E. H. Distribution control enables efficient reduced-dimensional perovskite LEDs. *Nature* **2021,** 599 (7886), 594-598, DOI: 10.1038/s41586-021-03997-z.
(43) Han, M. G.; Im, S. S. X-ray photoelectron spectroscopy study of electrically conducting polyaniline/polyimide blends. *Polymer* **2000,** 41 (9), 3253-3262, DOI: 10.1016/s0032-3861(99)00531-5.

(44) Ren, Z.; Xiao, X.; Ma, R.; Lin, H.; Wang, K.; Sun, X. W.; Choy, W. C. H. Hole transport bilayer structure for quasi-2D perovskite based blue light-emitting diodes with high brightness and good spectral stability. *Adv. Funct. Mater.* **2019,** 29 (43), 1905339, DOI: 10.1002/adfm.201905339.
(45) Li, B.; Zhen, J.; Wan, Y.; Lei, X.; Liu, Q.; Liu, Y.; Jia, L.; Wu, X.; Zeng, H.; Zhang, W.; Wang, G. W.; Chen, M.; Yang, S. Anchoring fullerene onto perovskite film via grafting pyridine toward enhanced electron transport in high-efficiency solar cells. *ACS. Appl. Mater. Inter.* **2018,** 10 (38), 32471-32482, DOI: 10.1021/acsami.8b11459.
(46) Luo, B.; Pu, Y.-C.; Yang, Y.; Lindley, S. A.; Abdelmageed, G.; Ashry, H.; Li, Y.; Li, X.; Zhang, J. Z. Synthesis, optical properties, and exciton dynamics of organolead bromide perovskite nanocrystals. *J. Phys. Chem. C* **2015,** 119 (47), 26672-26682, DOI: 10.1021/acs.jpcc.5b08537.
(47) Zhou, N.; Shen, Y.; Li, L.; Tan, S.; Liu, N.; Zheng, G.; Chen, Q.; Zhou, H. Exploration of crystallization kinetics in quasi two-dimensional perovskite and high performance solar cells. *J. Am. Chem. Soc.* **2018,** 140 (1), 459-465, DOI: 10.1021/jacs.7b11157.
(48) Duan, C.; Yu, Y.; Yang, P.; Zhang, X.; Li, F.; Li, L.; Xi, H. Engineering new defects in MIL-100(Fe) via a mixed-ligand approach to effect enhanced volatile organic compound adsorption capacity. *Ind. Eng. Chem. Res.* **2019,** 59 (2), 774-782, DOI: 10.1021/acs.iecr.9b05751.
(49) Kohn, W.; Sham, L. J. Self-consistent equations including exchange and correlation effects. *Phys. Rev.* **1965,** 140 (4A), A1133-A1138, DOI: 10.1103/PhysRev.140.A1133.
(50) Liu, L.; Xu, K.; Vickers, E. T.; Allen, A. L.; Li, X.; Peng, L.; Zhang, J. Z. Varying the concentration of organic acid and amine ligands allows tuning between quantum dots and magic-sized clusters of $CH_3NH_3PbBr_3$ perovskite: Implications for photonics and energy conversion. *ACS. Appl. Nano. Mater.* **2020,** 3 (12), 12379-12387, DOI: 10.1021/acsanm.0c02894.
(51) Ono, L. K.; Liu, S.; Qi, Y. Reducing detrimental defects for high-performance metal halide perovskite solar cells. *Angew. Chem. Int. Ed.* **2020,** 59 (17), 6676-6698, DOI: 10.1002/anie.201905521
10.1002/ange.201905521.
(52) Han, B.; Yuan, S.; Cai, B.; Song, J.; Liu, W.; Zhang, F.; Fang, T.; Wei, C.; Zeng, H. Green perovskite light-emitting diodes with 200 hours stability and 16% efficiency: Cross-linking strategy and mechanism. *Adv. Funct. Mater.* **2021**, 2011003, DOI: 10.1002/adfm.202011003.
(53) Fang, Z.; Shang, M.; Hou, X.; Zheng, Y.; Du, Z.; Yang, Z.; Chou, K.-C.; Yang, W.; Wang, Z. L.; Yang, Y. Bandgap alignment of α-$CsPbI_3$ perovskites with synergistically enhanced stability and optical performance via B-site minor doping. *Nano Energy* **2019,** 61, 389-396, DOI: 10.1016/j.nanoen.2019.04.084.
(54) Králik, M. Adsorption, chemisorption, and catalysis. *Chemical Papers* **2014,** 68 (12), DOI: 10.2478/s11696-014-0624-9.

(55) Koh, W.-k.; Park, S.; Ham, Y. Phosphonic acid stabilized colloidal $CsPbX_3$(X=Br, I) perovskite nanocrystals and their surface chemistry. *ChemistrySelect* **2016,** 1 (13), 3479-3482, DOI: 10.1002/slct.201600809.
(56) Woo, J. Y.; Lee, S.; Lee, S.; Kim, W. D.; Lee, K.; Kim, K.; An, H. J.; Lee, D. C.; Jeong, S. Air-stable PbSe nanocrystals passivated by phosphonic acids. *J. Am. Chem. Soc.* **2016,** 138 (3), 876-83, DOI: 10.1021/jacs.5b10273.
(57) Fang, Z.; Wang, E.; Chen, Y.; Hou, X.; Chou, K. C.; Yang, W.; Chen, J.; Shang, M. Wurtzite aln(0001) surface oxidation: hints from Ab initio calculations. *ACS. Appl. Mater. Inter.* **2018,** 10 (36), 30811-30818, DOI: 10.1021/acsami.8b08242.
(58) Fang, Z.; Shang, M.; Zheng, Y.; Zhang, T.; Du, Z.; Wang, G.; Duan, X.; Chou, K.-C.; Lin, C.-H.; Yang, W.; Hou, X.; Wu, T. Organic intercalation engineering of quasi-2D Dion–Jacobson α-$CsPbI_3$ perovskites. *Mater. Horiz.* **2020,** 7 (4), 1042-1050, DOI: 10.1039/c9mh01788g.
(59) Cai, J.; Hou, X.; Fang, Z.; Wang, E.; Feng, J.; Chen, J.; Liang, T.; Bei, G. Ab initio calculation of the evolution of $[SiN_{4-n}O_n]$ tetrahedron during $\beta$-$Si_3N_4$(0001) surface oxidation. *J. Am. Ceram. Soc.* **2019,** 103 (4), 2808-2816, DOI: 10.1111/jace.16922.
(60) Palazon, F.; Di Stasio, F.; Lauciello, S.; Krahne, R.; Prato, M.; Manna, L. Evolution of $CsPbBr_3$ nanocrystals upon post-synthesis annealing under an inert atmosphere. *J. Mater. Chem. C* **2016,** 4 (39), 9179-9182, DOI: 10.1039/c6tc03342c.
(61) Liu, M. M.; Wan, Q.; Wang, H. M.; Carulli, F.; Sun, X. C.; Zheng, W. L.; Kong, L.; Zhang, Q.; Zhang, C. Y.; Zhang, Q. G.; Brovelli, S.; Li, L. Suppression of temperature quenching in perovskite nanocrystals for efficient and thermally stable light-emitting diodes. *Nat. Photonics* **2021,** 15 (5), 379-385, DOI: 10.1038/s41566-021-00766-2.
(62) Xing, K.; Cao, S.; Yuan, X.; Zeng, R.; Li, H.; Zou, B.; Zhao, J. Thermal and photo stability of all inorganic lead halide perovskite nanocrystals. *Phys. Chem. Chem. Phys.* **2021,** 23 (32), 17113-17128, DOI: 10.1039/d1cp02119b.
(63) Rowland, C. E.; Liu, W.; Hannah, D. C.; Chan, M. K. Y.; Talapin, D. V.; Schaller, R. D. Thermal stability of colloidal InP nanocrystals: small inorganic ligands boost high-temperature photoluminescence. *ACS nano* **2014,** 8 (1), 977-985, DOI: 10.1021/nn405811p.
(64) Yuan, X.; Ji, S.; De Siena, M. C.; Fei, L.; Zhao, Z.; Wang, Y.; Li, H.; Zhao, J.; Gamelin, D. R. Photoluminescence temperature dependence, dynamics, and quantum efficiencies in $Mn^{2+}$-doped $CsPbCl_3$ perovskite nanocrystals with varied dopant concentration. *Chem. Mater.* **2017,** 29 (18), 8003-8011, DOI: 10.1021/acs.chemmater.7b03311.
(65) Pistor, P.; Burwig, T.; Brzuska, C.; Weber, B.; Fränzel, W. Thermal stability and miscibility of co-evaporated methyl ammonium lead halide ($MAPbX_3$, X = I, Br, Cl) thin films analysed by in situ X-ray diffraction. *J. Mater. Chem. A* **2018,** 6 (24), 11496-11506, DOI: 10.1039/c8ta02775g.
(66) Nguyen, H. D.; Lin, C. C.; Liu, R. S. Waterproof alkyl phosphate coated fluoride phosphors for optoelectronic materials. *Angew. Chem. Int. Ed.* **2015,** 54 (37), 10862-6, DOI: 10.1002/anie.201504791.

(67) Chen, Q.; Fu, H.; Wang, N.; Gao, F.; Yang, W.; Liu, W.; Zheng, J. Enhanced thermal stability of $MAPbBr_3$ nanocrystals by ligand modification. *Mater. Res. Bull.* **2023,** 157, 112009, DOI: 10.1016/j.materresbull.2022.112009.
(68) Kresse, G.; Furthmuller, J. Efficient iterative schemes for ab initio total-energy calculations using a plane-wave basis set. *Phys. Rev. B* **1996,** 54 (16), 11169-11186, DOI: 10.1103/physrevb.54.11169.
(69) Perdew, J. P.; Burke, K.; Ernzerhof, M. Generalized gradient approximation made simple. *Phys. Rev. Lett.* **1996,** 77 (18), 3865-3868, DOI: 10.1103/PhysRevLett.77.3865.

## Table of Contents synopsis

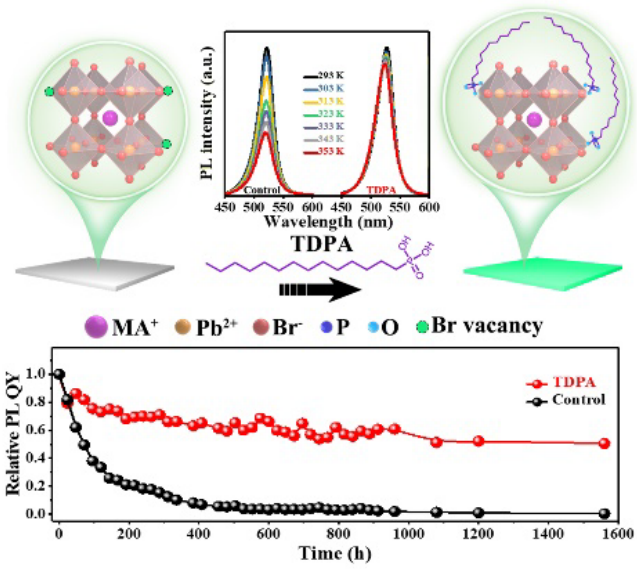


Controllable in-situ grown organic-inorganic hybrid perovskite nanocrystals in polymer with profoundly enhanced hygrothermal stability were reported. They exhibited robust stability with almost 100% retention of initial PL QY after exposure in air at 333 K for 1800 h, and 88.6% of initial PL intensity was retained once the temperature is increased from 293 to 353 K. Moreover, their PL QY can be maintained above 50% over 1560 h (65 days) under 333 K and 90% humidity.